Macromolecules
COMMUNICATION TO THE EDITOR

Macromolecules **2010**, *43*, 1169–1174 **1169**
DOI: 10.1021/ma902477h

Understanding the Influence of Morphology on Poly(3-hexylselenothiophene):PCBM Solar Cells

Amy M. Ballantyne, Toby A. M. Ferenczi, Mariano Campoy-Quiles, Tracey M. Clarke, Andrea Maurano, Kien Hon Wong, Weimin Zhang, Natalie Stingelin-Stutzmann, Ji-Seon Kim, Donal D. C. Bradley, James R. Durrant, Iain McCulloch, Martin Heeney, and Jenny Nelson*

Imperial College London, London SW7 2AZ, United Kingdom

Steve Tierney and Warren Duffy

Merck Chemicals, Chilworth Science Park, University Parkway, Southampton SO16 7QD, United Kingdom

Christian Mueller and Paul Smith

Department of Materials, ETH Zurich, Switzerland

Received November 9, 2009
Revised Manuscript Received January 3, 2010

Introduction. In organic bulk-heterojunction (BHJ) solar cells, a nanoscale blend of donor and acceptor materials (such as polymer:fullerene, polymer:nanocrystal, or polymer:polymer blends) is used to provide a high interfacial area at which photogenerated excitons can dissociate to yield separate charges. Efficient conversion of absorbed photons into photocurrent requires sufficiently intimate mixing of the donor and acceptor phases such that photogenerated excitons can easily find an interface as well as a sufficiently large thermodynamic driving force for charge separation at the interface. At the same time, efficient transport of separated charges toward the electrodes requires a certain degree of phase segregation between the two materials to enable ordered molecular packing within each phase and also minimize interfacial recombination. The optimum microstructure should thus be a compromise between intimate mixing and complete segregation of the two phases.

Poly(3-hexylthiophene) (P3HT):[6,6]-phenyl-C61-butyric acid methyl ester (PCBM) is a well-studied BHJ blend with some of the highest reported solar cell efficiencies (4−5%).[1−3] High photocurrents are obtained only after a thermal annealing process which leads to crystallization of the polymer and formation of aggregates of PCBM (which may be up to micrometers in size). In comparison to other polymer:fullerene systems, the annealed P3HT:PCBM films show excellent phase separation to produce domains comprised mostly of a single constituent, as evidenced e.g. by the increased photoluminescence (PL) from fullerene-rich films that is observed upon thermal annealing.[2]

We have recently reported studies of BHJ solar cells made from poly(3-hexylthiophene) (P3HS), a selenophene analogue of P3HT that has a lower optical gap than P3HT (1.6 eV compared to 1.9 eV) but a similar ionization potential level (4.8 eV).[4] According to the model presented by Scharber et al.,[5] P3HS:PCBM blend devices should, as a result of the lower optical gap and similar HOMO energy, be capable of producing higher power conversion efficiencies than P3HT:PCBM devices, assuming that equally good fill factor (FF) and external quantum efficiency (EQE) are obtained. It was observed that replacing P3HT with P3HS in polymer:PCBM blend BHJ solar cells led to a higher short-circuit current density, J_{sc} (of 6.5 cf. 4.8 mA cm^{-2} under 50 mW cm^{-2} illumination), as expected from the lower optical gap, and similar open-circuit voltage, V_{oc}, as expected from the similar ionization potential of P3HS and P3HT. However, the photocurrent EQE was much lower for the P3HS-based device, in spite of the larger photocurrent, and the FF was much reduced (40% compared to 55% for P3HT), leading to a lower overall power conversion efficiency of 2.7% compared to 3.0% for devices measured under the same conditions.[6]

The P3HS-based blend films and devices differ only from the P3HT-based systems in the polymer used: devices have the same structure, same blend film composition, and similar processing conditions were followed during device fabrication. The polymers differ primarily in the heteroatom (Se versus S) but also in the molecular weight (P3HS: M_n = 81 kDa; P3HT: M_n = 13 kDa). The similar HOMO energies of the polymers mean that the polymer−anode interface should be energetically similar. Therefore, we can eliminate some parameters that commonly affect FF, such as differences in series resistance resulting from choice of contacts.

We have identified several factors that could be responsible for the disappointing performance of the P3HS:PCBM devices: poor charge mobility, poor charge pair separation efficiency, and nonoptimum vertical phase distribution, affecting electrode selectivity. All of these effects are influenced by the blend film microstructure. For example, suboptimum microstructure may lead to poor mobility, both through the effect of phase segregation on percolation, affecting electron mobility,[7] and the disruptive effect of PCBM on polymer chain packing, which can affect hole mobility by a reduction in conjugation length (affecting intrachain transport) or poor packing of neighboring segments (affecting interchain transport).[8] Low charge mobility has been shown both by theory[9] and experiment[10] to reduce charge collection efficiency by allowing bimolecular recombination to compete more effectively with charge transport to the electrodes.

We have used differential scanning calorimetry (DSC), Raman imaging, optical microscopy, and X-ray diffraction (XRD) to probe and compare the microstructure of P3HS:PCBM and P3HT:PCBM blend films. The studies indicate that although the polymer phase is highly crystalline in each case, the P3HS domains in the P3HS:PCBM blend films appear to be less pure than the P3HT domains in the P3HT:PCBM films. Finally, transient photovoltage (TPV) measurements were used to study the effect of the detected changes in blend film microstructure on charge recombination kinetics.

Results and Discussion. DSC scans of P3HS:PCBM binary blends of different composition are shown in Figure 1a, and the resulting phase diagram is shown in Figure 1b. The P3HS:PCBM blends display a simple eutectic phase behavior similar to that reported previously for the P3HT:PCBM binary.[11] The eutectic composition for the P3HS:PCBM system is around 60 wt % P3HS, close to that found for P3HT:PCBM blends, and the eutectic temperature is

*To whom correspondence should be addressed. E-mail: jenny.nelson@imperial.ac.uk.

Published on Web 01/13/2010

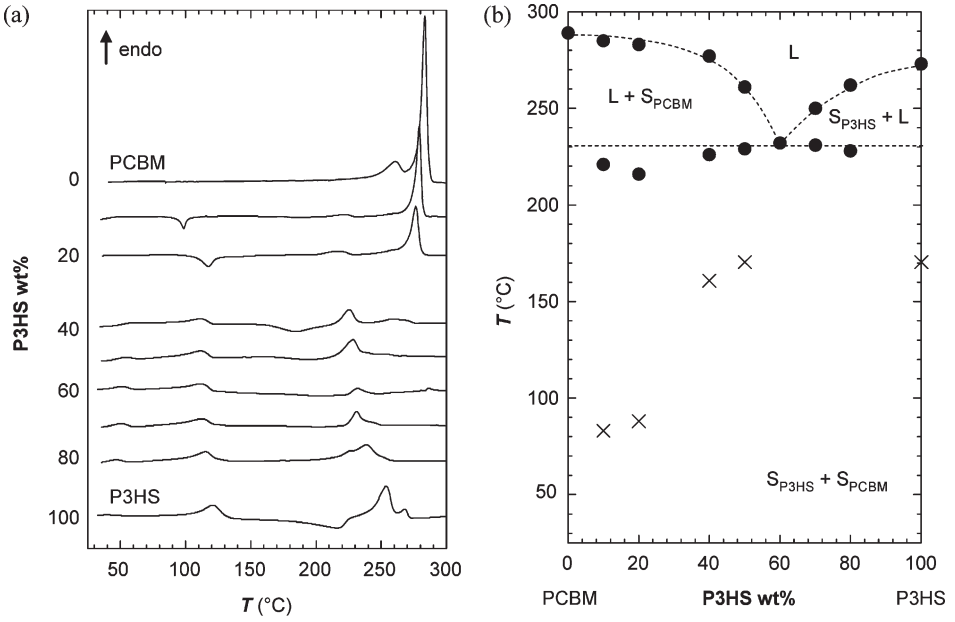

Figure 1. (a) Differential scanning calorimetry (DSC) heating thermograms and (b) corresponding (nonequilibrium) temperature/composition diagram of the P3HS:PCBM system, which features a simple eutectic phase behavior (peak eutectic temperature, $T_e \approx 230$ °C; eutectic composition, $c_e \approx 65$ wt % P3HS). L = liquid phase and S = solid phase. The crosses represent the onset of crystallization.

observed to be at ~230 °C. Clearly, in the solid state, the crystalline fractions of P3HT and PCBM phase segregate. However, we stress that we cannot deduce details of the degree of phase separation in the amorphous fractions of the two components from thermal analysis. Strictly speaking, we are dealing with at least a quasi-ternary system comprised of the small molecular compound, the crystalline polymer fraction, and the amorphous polymer phase, in which part of the small molecular species may be "dissolved".

P3HT:PCBM and P3HS:PCBM films were therefore imaged using micro-Raman spectroscopy mapping in order to compare microstructure and phase separation (Figure 2). Micro-Raman mapping allows the relative composition to be inferred from the strength of characteristic Raman peaks in order to build up a two-dimensional spatial map of composition.[12,13] The technique also reveals variations in polymer chain conformation through shifts in the position and changes in the relative intensity of the Raman peaks.[14,15] In Figure 2, the bright color represents the intensity of the Raman mode monitored at 1416 cm^{-1}, characteristic of the C=C stretch mode of the polymer, while the dark patches indicate the absence of that mode and were shown by confocal fluorescence microscopy to be PCBM-rich domains, rather than voids in the films. The as-spun P3HS:PCBM and P3HT:PCBM blend films (Figure 2a,b) appear to be of similar nature in that they both show good mixing of the polymer and fullerene. More significant mixing is evident after the upper part of each film (a layer about 20 nm thick) has been etched away (Figure 2c,d) where the films appear smooth without any distinctive phase separation.

Figures 2e,f display the P3HS:PCBM and P3HT:PCBM blend films after annealing and etching. A significantly coarser phase separation between polymer and PCBM, with larger dark domains, is observed upon thermal annealing for both systems. However, assuming that the Raman scattering cross sections of P3HT and P3HS are similar, the lower contrast between the bright and dark regions in the P3HS:PCBM blend film than for the P3HT:PCBM film suggests that the phase separation of P3HS and PCBM into domains of neat components is less complete than it is for P3HT and PCBM. Such an effect could result from a larger amorphous fraction in the case of P3HS than P3HT polymer.

The notion that, after annealing, the polymer-rich domains are less "polymer-rich" in the case of P3HS:PCBM films than in P3HT:PCBM films is also supported by confocal fluorescence maps of annealed, etched blend films (Figure 3). Emission detected from PCBM-rich domains shows the characteristic emission spectrum of PCBM peaking at 720 nm[16] while the PCBM-poor domains are dominated by polymer emission. Comparison of the relative strength of polymer emission from a PCBM-poor domain with that of PCBM emission from a PCBM-rich aggregate (Figure 3) shows that the polymer emission relative to the fullerene emission is weaker for the P3HS:PCBM than for the P3HT:PCBM blend. This is consistent with a larger concentration of finely dispersed PCBM in the P3HS polymer (i.e., a solid solution is formed), leading to more efficient PL quenching after annealing. In the case of P3HT:PCBM blends, the less efficient quenching of polymer emission that is observed after annealing can be explained in terms of strong phase segregation during annealing, leading to the formation of "purer" polymer domains,[2] also discussed below.

Comparison of optical micrographs of annealed P3HT:PCBM and P3HS:PCBM blend films (Figure 4) also indicate that the polymer-rich phase contains more finely dispersed PCBM in the case of P3HS:PCBM than P3HT:PCBM blend films. Despite the fact that both films contain the same weight fraction of PCBM, the P3HS blend film shows smaller and fewer PCBM crystals than the P3HT blend film. This difference is unlikely to result from the different eutectic compositions for the two blends, since the lower eutectic composition (in terms of the polymer) for the P3HS:PCBM than for the P3HT:PCBM blend would normally lead to a larger, rather than a smaller fraction of PCBM primaries in the case of P3HS:PCBM. However, our results are consistent with a report by Woo et al.,[17] who observed larger and more numerous PCBM crystals upon annealing of P3HT:PCBM blend films made from P3HT polymer of higher regioregularity. That result could be explained by the tendency of

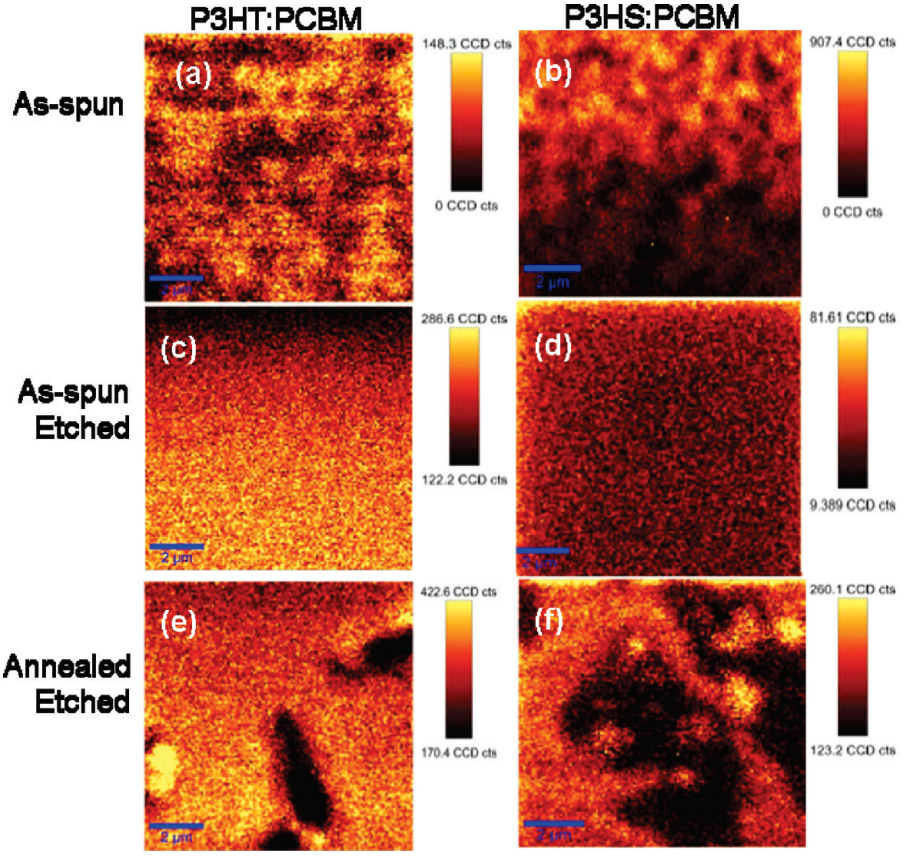

Figure 2. Raman images (10 μm × 10 μm) of (a, c, e) P3HT:PCBM (50 wt % PCBM) and (b, d, f) P3HS:PCBM (50 wt % PCBM) films (a, b) as-spun, (c, d) as spun and etched, and (e, f) annealed and etched. Raman intensities were collected at 1400−1480 cm^{-1} for P3HT and 1380−1460 cm^{-1} for P3HS under 633 nm excitation. Scanning pixel size: 128 × 128. Integration time: 0.1 s (except 0.3 s for (b)). 15−20 nm of the films was etched away using plasma etcher. No significant changes in the Raman spectra were found due to etching.

highly regioregular P3HT to crystallize, which results in a strong phase segregation with PCBM forming relatively large crystalline domains. With P3HT of lower regioregularity that does not crystallize as readily, smaller P3HT crystals were formed, indicating that more PCBM remains finely dispersed, most likely in the amorphous fractions of the polymer.[17] In the present case, where there is the same polymer: PCBM ratio in both the P3HS:PCBM and P3HT:PCBM blend films, the fact that fewer and smaller PCBM crystals are observed in the P3HS-based film indicates that there is still a significant amount of PCBM finely dispersed within the polymer-rich domains in the P3HS:PCBM blend film.

In order to compare the degree of polymer crystallinity in the P3HS:PCBM and P3HT:PCBM blend films, we have analyzed the two blends by wide-angle X-ray diffraction. Because the polymer structures are similar, with the same length side chain and similar regioregularity, we can compare the breadth of the diffraction peak corresponding to the interchain, intraplane (100) spacing (Figure 5a). The smaller height:width ratio of the diffraction feature at $2\theta \sim 5.5°$ (corresponding to d-spacing of 1.6 nm between polymer chains) indicates a lower degree of crystallinity in the P3HS blend film than the P3HT blend film.[2] A lower degree of crystallinity in P3HS is also consistent with the lower hole mobility in P3HS, as measured by time-of-flight (ToF) photoconductivity (Figure 5b). Although annealing the pristine P3HS film improves TOF hole mobility substantially,[6] hole mobility in annealed P3HS films is still an order of magnitude less than in P3HT (2×10^{-5} cm^2 V^{-1} s^{-1} vs 2×10^{-4} cm^2 V^{-1} s^{-1}). The lower hole mobility in P3HS compared to P3HT is likely to reduce charge collection efficiency, and hence FF, by increasing the probability of bimolecular recombination during charge transit.

The lower crystallinity of P3HS compared to that of P3HT could, in principle, result from a lower regioregularity (RR) or higher molecular weight (MW) of the polymer. RR is unlikely to be hindering crystallization as synthetic characterization data of the polymers shows that the P3HS sample used here has a slightly higher RR (97%) than the P3HT (94%). The difference in MW (13 kDa for P3HT vs 81 kDa for P3HS) could, in principle, influence crystallinity.[18] Recent studies by Stingelin-Stutzmann et al.[19] indicate that the crystallinity of P3HT is reduced significantly for large molecular weights (MW > 120 kDa). Lower polymer crystallinity for P3HS:PCBM than P3HT:PCBM blends could be partially responsible for the poorer device performance. However, reducing the MW of the P3HS polymer did not result in improved performance. A lower MW P3HS sample (MW = 41 kDa, RR = 95%) was tested, but the resulting devices gave significantly worse J_{sc}, V_{oc}, FF, and PCE (1.3 mA cm^{-2}, 0.34 V, 17%, and 0.15%, respectively) than the higher MW P3HS-based devices.

Reduced capability of the P3HS to crystallize could also be caused by several factors. These include the higher MW of the P3HS polymer and the possibility of different packing of the side chains due to the effect of the heteroatom. To study this, we have measured Raman spectra of pristine P3HS and P3HT films (Figure 6). It was found that replacement of S by Se leads to both (i) a softening of the main in-plane ring skeleton modes (1442 to 1417 cm^{-1} [symmetric C=C stretch mode] and 1376 to 1358 cm^{-1} [C−C stretch mode]) and

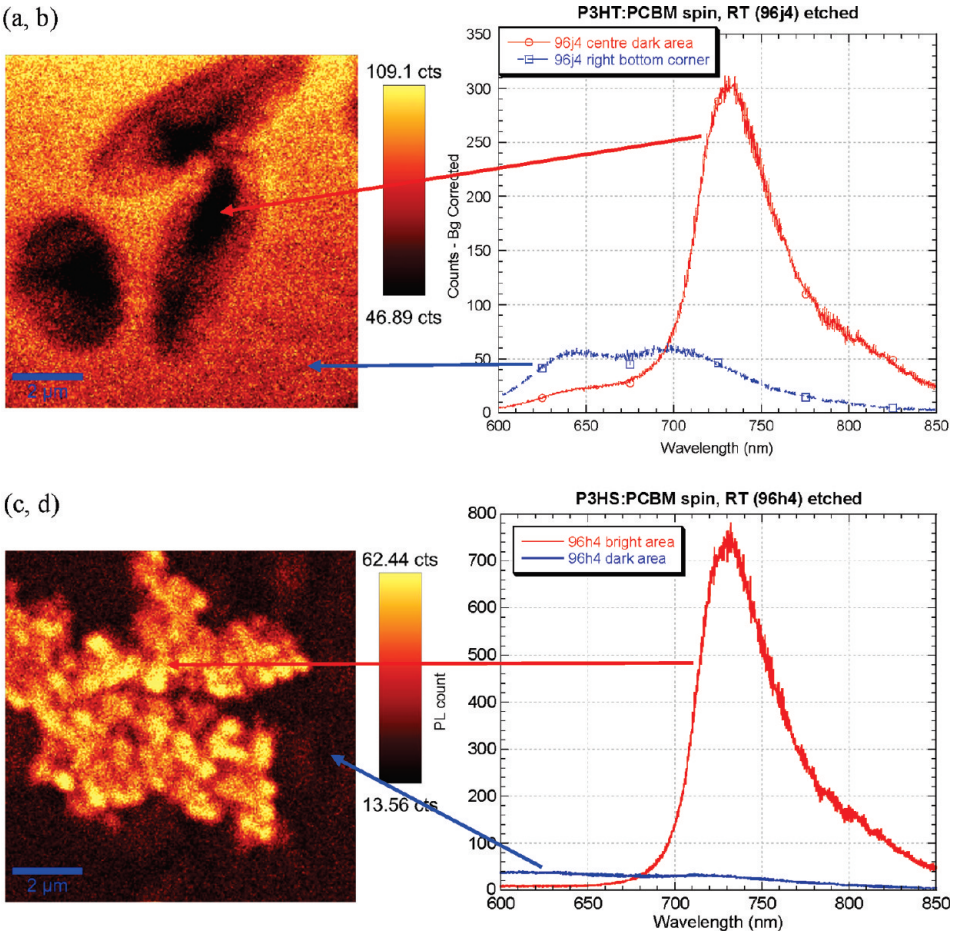

Figure 3. Confocal fluorescence images (10 μm × 10 μm) (a, c) and fluorescence spectra (b, d) for annealed, etched blend films of (a, b) P3HT:PCBM (50 wt % PCBM) and (c, d) P3HS:PCBM (50 wt % PCBM) films. Images were obtained by summing the total spectral pixel intensity from 600 to 850 nm. Excitation: 405 nm. Scanning pixel size: 256 × 256. Integration: 0.005 s. Note that the bright areas in fluorescence images are polymer-rich in P3HT:PCBM film and PCBM-rich in P3HS:PCBM film, indicating relatively stronger PL quenching in the latter case.

(ii) an increase in the intensity of inter-ring C−C stretch modes at 1173−1203 cm^{-1}. The observed softening of the main Raman peaks is consistent both with higher MW of the P3HS polymer, similar to that which has been observed in other fluorene based polymers,[15] and with different bond lengths due to the replacement of S with the heavier Se atom. The data thus indicate that the blend film microstructures differ in the amount of PCBM dispersed in the polymer (most likely in the amorphous fraction), resulting from the different ability for each polymer to crystallize within the blend film. As explained above, a lower degree of crystallinity can account for a lower degree of purity in the polymer phase after thermal annealing.

A lower degree of "purity" in the separate phases is likely to influence device performance by increasing the rate of bimolecular recombination through the larger interface between the two materials. To investigate this, we have used the transient photovoltage technique (TPV) to study the rate of charge pair recombination at open circuit.[20] Measurements were made at open circuit under a white bias light while optical perturbation was used to create a voltage transient. At open circuit, photogenerated charge carriers are forced to remain in the device active layer or the electrodes, and the TPV decay can therefore be used to monitor the loss kinetics.

TPV data comparing traces for blend devices of P3HT:PCBM and P3HS:PCBM measured at the same charge carrier density (~3 × 10^{16} cm^{-3}) are shown in Figure 7. It is clear that at the same charge density the lifetime for P3HS blend is about 10 times shorter than that of P3HT blends. This is consistent with our studies of microstructure which show that the polymer-rich domains in P3HS:PCBM blend films are less polymer-pure than those in P3HT:PCBM blend films. This higher rate of recombination will enhance the competition between recombination and transport in P3HS:PCBM vs P3HT:PCBM and is likely to contribute to the lower FF and, potentially, lower the EQE and V_{OC}, as discussed elsewhere.[21] We note the EQE is also likely to be influenced by a lower charge separation yield as determined using transient optical spectroscopy.[22]

Conclusions. We have studied the microstructure, charge transport, and charge recombination dynamics in blend films of P3HS:PCBM in comparison with P3HT:PCBM in an attempt to identify the reasons for the poorer performance in P3HS:PCBM photovoltaic devices. We have found that, in spite of the high crystallinity of P3HS as indicated by DSC, P3HS:PCBM blend films show a lower degree of crystallinity than P3HT:PCBM according to XRD measurements. As a consequence, it seems that larger fractions of PCBM can be dissolved in the polymer, as deduced from optical microscopy, Raman, and fluorescence mapping. This lower crystallinity could be caused by the higher molecular weight of the P3HS polymer compared to the P3HT polymer sample used in this study. The lower degree of phase segregation is likely to contribute to the faster recombination kinetics observed in the P3HS:PCBM than in P3HT:PCBM blend devices, and this may be reinforced by lower hole

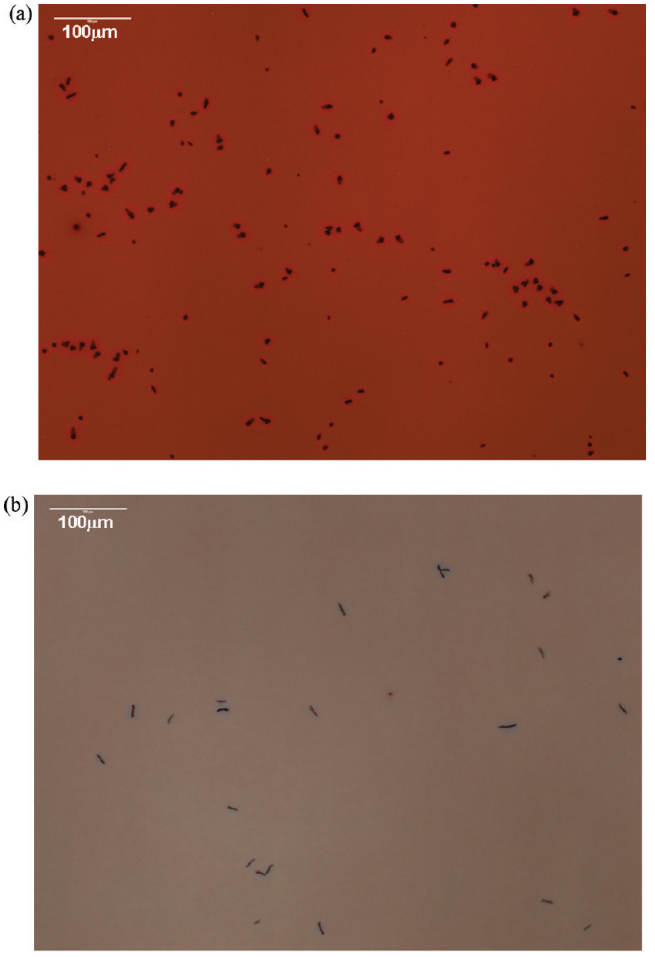

Figure 4. Optical images of (a) P3HT:PCBM (50 wt % PCBM) and (b) P3HS:PCBM (50 wt % PCBM) blend films after thermal annealing.

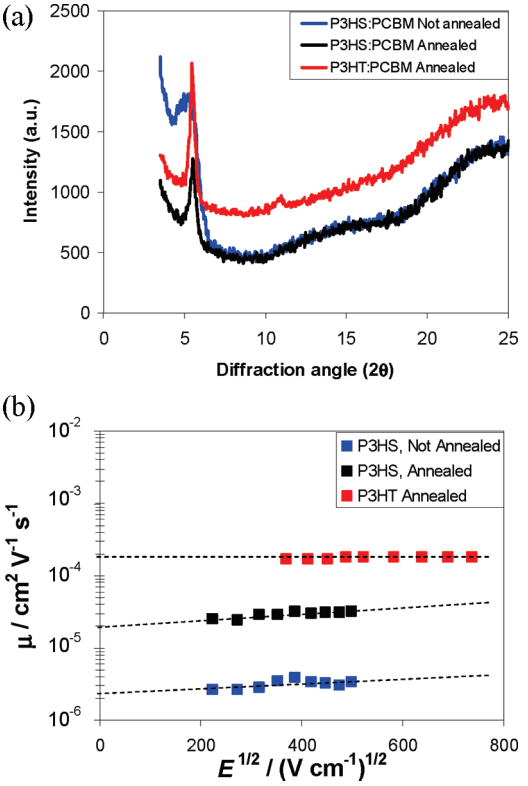

Figure 5. (a) XRD spectra of PCBM blend films of P3HT (red) and P3HS before (blue) and after (black) annealing. (b) Electric field dependence of time-of-flight hole mobility for pristine P3HT films (red) and P3HS films before (blue) and after (black) annealing.

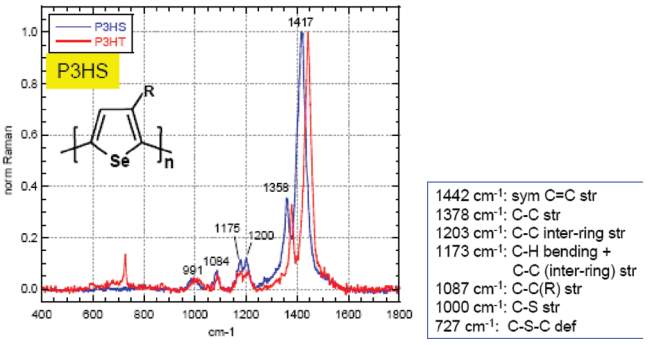

Figure 6. (a) Raman spectra of P3HT (red) and P3HS (blue). The assignments are made for P3HT[23,24] and numbers on the graph for P3HS. Excitation at 633 nm.

mobility in P3HS than P3HT. The study shows that fine control of blend film microstructure through the self-organizing properties of the component materials is essential to realize the potential of new organic photovoltaic materials.

Experimental Section. P3HS M_w = 147 kDa; M_n = 81 kDa, regioregularity >97%) and P3HT (M_w = 18 KDa, M_n = 13 kDa, regioregularity >94.4%) were prepared by Merck Chemicals Ltd. Both polymer and polymer:PCBM (API Services, Inc.) blend solutions were prepared using chlorobenzene (BDH Laboratory Supplies) and stirred for 24 h (while heating at 80 °C in the case of P3HS solutions) to fully dissolve the polymer. P3HT:PCBM and P3HS:PCBM blend films (1:1) were spin-coated onto quartz substrates from warm (60−70 °C) solutions. Because of low solubility of P3HS (and a tendency to precipitate out of solution at low temperatures), P3HS:PCBM films were spin-coated onto substrates that were 80 °C. It was previously found that P3HS:PCBM devices made using hot substrates performed better than devices prepared using room-temperature substrates.[6] All films were deposited in a clean room with a filtered air environment. Some blend films were thermally annealed at 140 °C for 30 min in a dry nitrogen environment. For micro-Raman spectroscopy and photoluminescence measurements, blend films were spin-coated on to quartz substrates as described above. For some samples, the top 15−20 nm of the organic blend film was removed by oxygen plasma etching at a plasma power of 100 W (for 4 min with an average etching rate of 3−4 nm/min for P3HT:PCBM films and for 2 min with an average etching rate of 10 nm/min for P3HS:PCBM films).[1] Differential scanning calorimetry (DSC) was conducted under nitrogen at a scan rate of 10 °C min^{-1} with a Mettler Toledo DSC822 instrument. The sample weight was ~10 mg. Eutectic transition temperatures were taken to be the peak maxima in the respective thermograms and complete dissolution of primary crystals as well as melting of the pure materials corresponds to end melting temperatures. For micro-Raman spectroscopy measurements, samples were excited in a 180° backscattering geometry by a 633 nm laser diode focused through a 100× objective in a WITec confocal Raman microscope. The Rayleigh scattered light was eliminated by an edge filter such that only the Raman scattered light dispersed by a grating was collected by a Peltier-cooled deep-depletion CCD detector. The Raman spectra were corrected for dark noise from the detector and fluorescent background from the polymers. XRD data were collected using a Philips

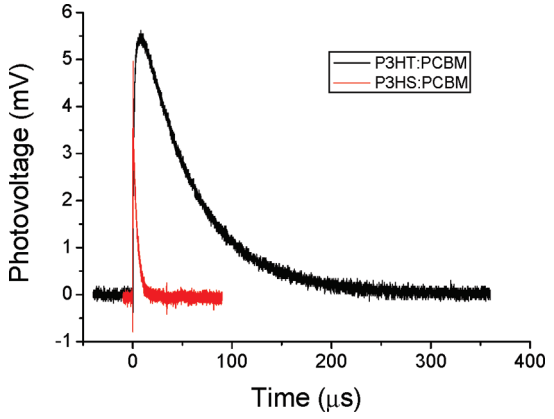

Figure 7. (a) Transient photovoltage traces of P3HT:PCBM (50 wt % PCBM) blend devices (black) in comparison with P3HS:PCBM blend devices (red) held at the same charge carrier density ($\sim 3 \times 10^{16}$ cm^{-3}).

PW1700 series automated powder diffractometer using Cu Kα radiation at 40 kV/40 mA with a secondary graphite crystal monochromator. TPV measurements were made at open circuit by connecting the device to the 1 MΩ input terminal of an oscilloscope. A white light was used to generate the open-circuit voltage (V_{oc}) while a nitrogen pumped-dye laser was used as the excitation source (wavelength of 620 nm, frequency of 4 Hz, pulse duration <1 ns) to create a small optical perturbation resulting in a voltage transient with an amplitude $V < V_{oc}$.

Acknowledgment. We thank the DTI Technology Program and BP Solar for financial support.

References and Notes

(1) Irwin, M. D.; Buchholz, B.; Hains, A. W.; Chang, R. P. H.; Marks, T. J. *Proc. Natl. Acad. Sci. U.S.A.* **2008**, *105*, 2783–2787.
(2) Kim, Y.; Cook, S.; Tuladhar, S. M.; Choulis, S. A.; Nelson, J.; Durrant, J. R.; Bradley, D. D. C.; Giles, M.; McCulloch, I.; Ha, C. S.; Ree, M. *Nat. Mater.* **2006**, *5*, 197–203.
(3) Li, G.; Shrotriya, V.; Huang, J. S.; Yao, Y.; Moriarty, T.; Emery, K.; Yang, Y. *Nat. Mater.* **2005**, *4*, 864–868.
(4) Heeney, M.; Zhang, W.; Crouch, D. J.; Chabinyc, M. L.; Gordeyev, S.; Hamilton, R.; Higgins, S. J.; McCulloch, I.; Skabara, P. J.; Sparrowe, D.; Tierney, S. *Chem. Commun.* **2007**, 5061–5063.
(5) Scharber, M. C.; Wuhlbacher, D.; Koppe, M.; Denk, P.; Waldauf, C.; Heeger, A. J.; Brabec, C. J. *Adv. Mater.* **2006**, *18*, 789.
(6) Ballantyne, A. M.; Chen, L. C.; Nelson, J.; Bradley, D. D. C.; Astuti, Y.; Maurano, A.; Shuttle, C. G.; Durrant, J. R.; Heeney, M.; Duffy, W.; McCulloch, I. *Adv. Mater.* **2007**, *19*, 4544.
(7) Tuladhar, S. M.; Poplavskyy, D.; Choulis, S. A.; Durrant, J. R.; Bradley, D. D. C.; Nelson, J. *Adv. Funct. Mater.* **2005**, *15*, 1171–1182.
(8) Mihailetchi, V. D.; Xie, H. X.; de Boer, B.; Koster, L. J. A.; Blom, P. W. M. *Adv. Funct. Mater.* **2006**, *16*, 699–708.
(9) Brabec, C. J.; Shaheen, S. E.; Fromherz, T.; Padinger, F.; Hummelen, J. C.; Dhanabalan, A.; Janssen, R. A. J.; Sariciftci, N. S. *Synth. Met.* **2001**, *121*, 1517–1520.
(10) Gadisa, A.; Zhang, F. L.; Sharma, D.; Svensson, M.; Andersson, M. R.; Inganas, O. *Thin Solid Films* **2007**, *515*, 3126–3131.
(11) Muller, C.; Ferenczi, T. A. M.; Campoy-Quiles, M.; Frost, J. M.; Bradley, D. D. C.; Smith, P.; Stingelin-Stutzmann, N.; Nelson, J. *Adv. Mater.* **2008**, *20*, 3510.
(12) Yim, K. H.; Zheng, Z. J.; Friend, R. H.; Huck, W. T. S.; Kim, J. S. *Adv. Funct. Mater.* **2008**, *18*, 2897–2904.
(13) Kim, J. S.; Ho, P. K. H.; Murphy, C. E.; Friend, R. H. *Macromolecules* **2004**, *37*, 2861–2871.
(14) Donley, C. L.; Zaumseil, J.; Andreasen, J. W.; Nielsen, M. M.; Sirringhaus, H.; Friend, R. H.; Kim, J. S. *J. Am. Chem. Soc.* **2005**, *127*, 12890–12899.
(15) Tsoi, W. C.; Lidzey, D. G. *J. Phys.: Condens. Matter* **2008**, *20*, 125213.
(16) van Duren, J. K. J.; Yang, X.; Loos, J.; Bulle-Lieuwma, C. W. T.; Sieval, A. B.; Hummelen, J. C.; Janssen, R. A. J. *Adv. Funct. Mater.* **2004**, *14*, 425–434.
(17) Woo, C. H.; Thompson, B. C.; Burnjoon, J. K.; Toney, M. F.; Frechet, J. M. J. *J. Am. Chem. Soc.* **2008**, *130*, 16324–16329.
(18) Brinkmann, M.; Rannou, P. *Adv. Funct. Mater.* **2006**, *17*, 101–108.
(19) Stingelin-Stutzmann, N. Private communication, **2009**.
(20) Shuttle, C. G.; O'Regan, B.; Ballantyne, A. M.; Nelson, J.; Bradley, D. D. C.; de Mello, J.; Durrant, J. R. *Appl. Phys. Lett.* **2008**, *92*, 093311.
(21) Maurano, A.; Hamilton, R.; Shuttle, C. G.; Nelson, J.; O'Regan, B. C.; McCulloch, I.; Durrant, J. R. Manuscript in submission.
(22) Clarke, T. M.; Ballantyne, A. M.; Nelson, J.; Bradley, D. D. C.; Durrant, J. R. *Adv. Funct. Mater.* **2008**, *18*, 1–7.
(23) Baibarac, M.; Lapkowski, M.; Pron, A.; Lefrant, S.; Baltog, I. *J. Raman Spectrosc.* **1998**, *29*, 825–832.
(24) Louarn, G.; Trznadel, M.; Buisson, J. P.; Laska, J.; Pron, A.; Lapkowski, M.; Lefrant, S. *J. Phys. Chem.* **1996**, *100*, 12532–12539.